International Journal of Solids and Structures 50 (2013) 511–518

Contents lists available at SciVerse ScienceDirect

International Journal of Solids and Structures

journal homepage: www.elsevier.com/locate/ijsolstr

Stress and displacement fields in soft cylindrical multilayers

Dong Wang, M.S. Wu *

School of Mechanical and Aerospace Engineering, Nanyang Technological University, 50 Nanyang Avenue, Singapore 639798, Singapore

ARTICLE INFO

Article history:
Received 28 February 2012
Received in revised form 9 October 2012
Available online 2 November 2012

Keywords:
Multilayered gels
Second-order elastic model
Dilatations

ABSTRACT

Multilayered gels play an important role in biomedical engineering as drug delivery vehicles, replacement tissues and bio-mimetic substrates for cell cultures. It has been established that the gel elasticity strongly influences the intended functionalities. In view of this, second-order elastic solutions for the stresses and displacements in cylindrical multilayered hydrogels subjected to various dilatation profiles are developed in this paper. The results emphasize the importance of nonlinearity in gel mechanics, and suggest the possibility of a rational selection of layer elasticities, layer thicknesses and dilatation profiles for improved mechanical responses such as maximum/minimum swelling and multiaxial stress states.

1. Introduction

Multilayered gels play a significant role in many biomedical applications as each layer can be imbued with distinct chemical and mechanical properties for various targeted functionalities. Such coherent multilayered gels are widely used in tissue engineering, controlled drug delivery and surface modifications. For instance, Schneider et al. (2001) developed multilayered spherical capsules with high mechanical stability and biocompatibility for the transportation of pancreatic islets. Johnson et al. (2010) also developed multilayered cylindrical hydrogels via an iterative solution dipping technique, resulting in layer thicknesses in the range of 150–650 μm. Facca et al. (2010) demonstrated the possibility of differentiation of stem cells to bone cells using multilayered capsules containing active growth factors.

It has been established that the elastic properties of hydrogels play a critical role in biomedical applications. For stem cell cultures in a hydrogel microenvironment, Engler et al. (2006) showed that the elastic stiffness of the hydrogel dictates cell lineage specification. For stiffnesses in the range of 0.1–1, 8–17 and 25–40 kPa that respectively mimic brain, muscle and bone elasticity, the stem cells developed primarily into neurogenic, myogenic and osteogenic cells, respectively. Indeed, hydrogel elasticity is well-recognized as a critical factor in the biomaterial design of microenvironments in tissue engineering. Marklein and Burdick (2010) showed that the morphology and proliferation of human mesenchymal stem cells were strongly affected by the hydrogel elasticity, and Kloxin et al. (2010) demonstrated the influence of microenvironment elasticity on the differentiation and migration of valvular interstitial cells.

In view of the importance of elasticity in biomaterial design and the lack of theoretical investigation into the influence of elastic nonlinearity on multilayer design, recent attempts have been made in this area of soft matter mechanics. Specifically, Wu and Kirchner (2010) investigated a second-order elasticity model on the basis of the work of Murnaghan (1951), and applied it to the study of a homogeneous gel under tension, torsion and shear, and subsequently Wu and Kirchner (2011) investigated the case of a homogeneous spherical capsule and showed the importance of nonlinearity in the soft matter response. More recently, Wang and Wu (2012) considered the case of a bilayer spherical capsule and investigated the role of layer inhomogeneity.

The choice of a second-order model for the present study is motivated by the following considerations. First and foremost, the second-order model adopted is generic for any nonlinear material. Since the gels and soft tissues are extremely diverse in composition, a generic rather than a specific model for describing material nonlinearity is preferred here. Second, the first-order model is routinely used to describe the linear elasticity of gels and soft tissues and the second-order model is a natural extension and improvement for describing the inherent material nonlinearity. Third, higher-order generic elasticity models have already been used to describe the mechanical behavior of gels and tissues. Other than the works of the authors mentioned above, Rénier et al. (2008) considered the experimental determination of the elastic constants in fourth-order elasticity for the modeling of soft solids, while Destrade et al. (2010) discussed the invariants for fourth-order transversely isotropic elasticity for the modeling of biological soft tissues. These works focus on the structure of the constitutive equations in higher-order elasticity.

In the present work, solutions for the displacements and stresses are developed for a multilayered cylindrical hydrogel using a second-order elasticity model. It should be noted that the model is second-order in terms of stresses but third-order in terms of

* Corresponding author. Tel.: +65 67905545.
E-mail address: mmswu@ntu.edu.sg (M.S. Wu).

0020-7683/$ - see front matter © 2012 Elsevier Ltd. All rights reserved.
http://dx.doi.org/10.1016/j.ijsolstr.2012.10.012

the strain invariants; the abovementioned works on fourth-order elasticity adopted the latter terminology. The multilayer is loaded by a dilatation profile, simulating chemical/drug concentration or temperature distribution. Higher-order elasticity theories or other nonlinear elastic models can also be used to solve the multilayer problem, but the second-order theory is adopted for its relative simplicity and the derivability of analytical solutions as demonstrated later.

Following this introduction, the second-order elastic model is reviewed and the problem of an N-layer cylinder is established in Section 2. General solutions are derived in Section 3. Numerical results highlighting the influence of nonlinearity, material dissimilarity, non-uniform layer thicknesses and dilatation profiles are presented and discussed in Section 4. A list of conclusions are given in Section 5.

2. Nonlinear elastic model for dilatations

2.1. Definition of problem

Fig. 1 shows an N-layered circular hydrogel cylinder with interfaces located at the radial coordinates $r = r_j$, $j = 1, N$. The layers are nonlinearly elastic, isotropic, and perfectly bonded to one another, but can be of dissimilar material compositions and thicknesses. The outermost surface of the hydrogel is assumed to be traction-free. The second-order elasticity theory of Murnaghan (1951) is used to model the elastic nonlinearity of the gel layers. Two second-order elastic constants λ_j, μ_j and three third-order elastic constants l_j, m_j, n_j, where $j = 1, N$, are used in this theory.

The cylinder is subjected to an axisymmetric dilatation profile, which can however fluctuate along r. For definiteness, step dilatation profiles are assumed, in which the dilatation in each layer is constant but it may vary from layer to layer. Physically, fluctuations such as temperature $T(r)$ and chemical concentration $c(r)$ result in a local dilatation field $\vartheta(r)$. The relation between T and ϑ or between c and ϑ is given by the coefficient of thermal expansion or the change in lattice parameter per unit concentration, respectively. However, it is not necessary to specify these relations in the elasticity problem. The field $\vartheta(r)$ is considered as the fluctuation loading, and may be controlled, as in the embedding of drugs, nucleic acids, nutrients and growth factors of various concentrations in the layers of sub-micrometer thicknesses. The objective is to derive the displacement field and the stress field under the dilatation loading. To facilitate the derivations, the second-order elastic model is briefly reviewed in Section 2.

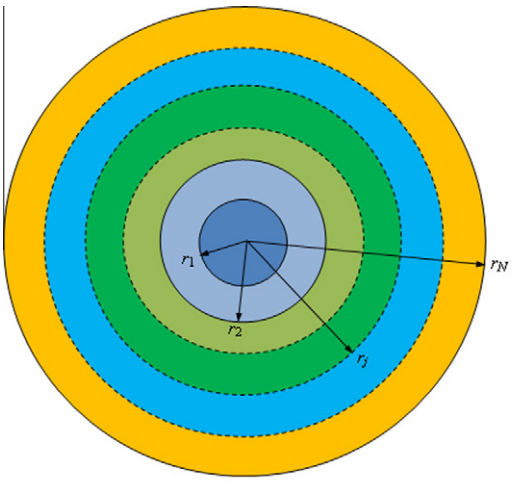

Fig. 1. A hydrogel cylinder composite consisting of N layers, with core radius r_1 and outermost radius r_N.

2.2. Second-order elastic model

The energy density W of Murnaghan (1951) is written as a function of the strain invariants J_1, J_2, J_3 of the Lagrangian strain $\mathbf{E}$:

$$W = \frac{\lambda + 2\mu}{2} J_1^2 - 2\mu J_2 + \frac{l + 2m}{3} J_1^3 - 2m J_1 J_2 + n J_3, \tag{2.1}$$

where λ, μ are the second-order and l, m, n the third-order elastic constants, respectively. In terms of the principal strains E_1, E_2 and E_3 of $\mathbf{E}$, the three strain invariants are:

$$J_1 = E_1 + E_2 + E_3, \quad J_2 = E_1E_2 + E_2E_3 + E_3E_1, \quad J_3 = E_1E_2E_3. \tag{2.2}$$

As the governing equation (the equilibrium equation) will be formulated in terms of displacements, the above strain invariants are expressed as a function of the radial displacement u_r and its derivative u_r' with respect to r. For a two-dimensional problem, J_1 and J_2 of Eq. (2.2) can be written as:

$$J_1 = k\left(u_r' + \frac{u_r}{r}\right) + \frac{1}{2}k^2\left[u_r'^2 + \left(\frac{u_r}{r}\right)^2\right], \quad J_2 = k^2\frac{u_r u_r'}{r}, \tag{2.3}$$

where k is introduced to keep track on the order of approximation of the theory. Note that J_3 does not appear, since the strain matrix $\mathbf{E}$ is two-dimensional rather than three dimensional. For this reason, the third-order elastic constant n in Eq. (2.1) will also not appear in the solutions.

For the linear and second-order approximations, only terms up to the first- and second-order of k are retained, respectively. Equation (2.3) can be derived from the form of $\mathbf{E}$ given below in Eq. (2.7). The stress in the undeformed coordinate system is written as the matrix product between the deformation gradient $\mathbf{J_a}$ and the derivative of the energy density with respect to the Lagrangian strain:

$$\mathbf{T} = \mathbf{J_a}\frac{\partial \mathbf{W}}{\partial \mathbf{E}}, \tag{2.4}$$

where

$$\frac{\partial W}{\partial \mathbf{E}} = \lambda J_1 \mathbf{I} + 2\mu\mathbf{E} + (lJ_1^2 - 2mJ_2)\mathbf{I} + 2mJ_1\mathbf{E}. \tag{2.5}$$

The deformation gradient $\mathbf{J_a}$ in Eq. (2.4) can be written in terms of u_r and u_r' as:

$$\mathbf{J_a} = \mathrm{diag}\left[1 + ku_r', 1 + \frac{ku_r}{r}\right], \tag{2.6}$$

as shown in Appendix A. The Lagrangian strain in Eq. (2.5) can then be expressed as:

$$\mathbf{E} = \frac{1}{2}(\mathbf{J_a^*J_a} - \mathbf{I}) = k\ \mathrm{diag}\left[u_r', \frac{u_r}{r}\right] + \frac{1}{2}k^2\mathrm{diag}\left[u_r'^2, \frac{u_r^2}{r^2}\right], \tag{2.7}$$

where $\mathbf{J_a^*}$ denotes the transpose of $\mathbf{J_a}$ and $\mathbf{I}$ is the identity matrix.

The equilibrium equation takes the following form:

$$\nabla \cdot \mathbf{T} + \rho\mathbf{F} = 0, \tag{2.8}$$

where ρ is the mass density and $\rho\mathbf{F}$ the body force per unit volume, while the boundary condition at the free surface of the hydrogel is:

$$\mathbf{T}d\mathbf{S} = 0, \tag{2.9}$$

where $d\mathbf{S}$ is the oriented surface element. Note that $\mathbf{T}$ is diagonal with the radial and polar components T_r and T_ϕ. Only the radial components of Eqs. (2.8) and (2.9) are relevant. These can be written as:

$$T_r' + \frac{1}{r}T_r - \frac{1}{r}T_\varphi = -\rho F_r, \tag{2.10}$$

where F_r is the radial component of **F**. An expression can be obtained for the body force as follows. According to Murnaghan (1951), a uniform dilatation ϑ causes a hydrostatic stress p given by:

$$p = -(3\lambda + 2\mu)\vartheta + \frac{1}{2}\left(\lambda + \frac{2}{3}\mu - 2l - \frac{2n}{9}\right)(3\vartheta)^2. \tag{2.11}$$

If ϑ varies with r, the variation of p with r is treated as a body force, i.e., ρF_r is written as the derivative of p with respect to r:

$$\rho F_r = -k\left(\lambda + \frac{2}{3}\mu\right)\frac{d(3\vartheta)}{dr} + k^2\left(\lambda + \frac{2}{3}\mu - 2l - \frac{2n}{9}\right)(3\vartheta)\frac{d(3\vartheta)}{dr}, \tag{2.12}$$

where k and k^2 separate out the first- and second-order terms. The expressions in Eqs. (2.10) and (2.12) complete the form of the governing equation. The derivation of the solutions is shown in Section 3.

3. Solutions

Eq. (2.10) is re-written in terms of u_r and u_r', where u_r is written as the sum of the first- and second- order displacements u and w:

$$u_r = u + kw, \tag{3.1}$$

and k keeps track of the approximation order. The total radial displacement is the direct sum of the first- and second-order displacements; k being merely a marker. From Eqs. (2.4) and (2.5), and noting that J_1 and J_2, $\mathbf{J_a}$ and **E** are all functions of u_r and u_r' according to Eqs. (2.3), (2.6), and (2.7), the expressions for T_r and T_θ can be written as:

$$T_r = kT_r^L + k^2 T_r^{NL}, \tag{3.2}$$

where the linear and nonlinear radial stresses T_r^L and T_r^{NL} are, respectively:

$$T_r^L = \lambda\left(u' + \frac{u}{r}\right) + 2\mu u', \quad T_r^{NL} = \begin{bmatrix} \lambda\left(\frac{3}{2}u'^2 + \frac{uu'}{r} + \frac{1}{2}\frac{u^2}{r^2}\right) \\ +3\mu u'^2 + l\left(u' + \frac{u}{r}\right)^2 + 2mu'^2 \\ +\lambda\left(w' + \frac{w}{r}\right) + 2\mu w' \end{bmatrix}, \tag{3.3}$$

and similarly

$$T_\varphi = kT_\varphi^L + k^2 T_\varphi^{NL}, \tag{3.4}$$

where the linear and nonlinear circumferential stresses T_φ^L and T_φ^{NL} are, respectively:

$$T_\varphi^L = \lambda\left(u' + \frac{u}{r}\right) + 2\mu\frac{u}{r}, \quad T_\varphi^{NL} = \begin{bmatrix} \lambda\left(\frac{1}{2}u'^2 + \frac{uu'}{r} + \frac{3}{2}\frac{u^2}{r^2}\right) \\ +3\mu\frac{u^2}{r^2} + l\left(u' + \frac{u}{r}\right)^2 + 2m\frac{u^2}{r^2} \\ +\lambda\left(w' + \frac{w}{r}\right) + 2\mu\frac{w}{r} \end{bmatrix}. \tag{3.5}$$

The total stresses are the direct sum of their linear and nonlinear components. The nonlinear stresses contain both u and w and their first-order derivatives. These stress expressions and the body force expression of Eq. (2.12) are substituted into the equilibrium equation, i.e., Eq. (2.10), to complete the displacement formulation.

Upon extracting the k term of the equilibrium equation, the first-order part can be written as:

$$(\lambda + 2\mu)\left(u'' + \frac{u'}{r} - \frac{u}{r^2}\right) = (3\lambda + 2\mu)\frac{d\vartheta}{dr}, \tag{3.6}$$

while the second-order equilibrium equation is associated with the k^2 term and can be written as:

$$\begin{aligned}(\lambda + 2\mu)\left(w'' + \frac{w'}{r} - \frac{w}{r^2}\right) = &-2(\lambda + 3\mu + 2m)\left(u'u'' + \frac{1}{2r}u'^2 - \frac{u^2}{2r^3}\right) \\ &- (\lambda + 2l)\left(u'' + \frac{u'}{r} - \frac{u}{r^2}\right)\left(u' + \frac{u}{r}\right) \\ &- \left(\lambda + \frac{2}{3}\mu - 2l - \frac{2n}{9}\right)9\vartheta\frac{d\vartheta}{dr}.\end{aligned} \tag{3.7}$$

These are second-order ordinary differential equations. Appropriate boundary conditions are applied. In the following subsections, the solutions for the stresses and radial displacement are derived. For convenience, subscripts j are attached to the symbols for the stresses and displacements in the jth-layer. It should be noted that in computing the stresses using Eqs. (3.3) and (3.5), u_r/r and u_r' should be replaced by $u_r/r - \vartheta$ and $u_r' - \vartheta$ respectively, as it is the difference between the fields that preserves the continuity of the body.

For each jth layer, it is assumed that the dilatation is a constant ϑ_j, $j = 1, N$. Substituting $\vartheta = \vartheta_j$ into the first-order governing equation (Eq. (3.6)), the linear displacement solutions can be obtained in the analytical form of a power law:

$$u_j = A_j r + \frac{B_j r_{j-1}^2}{r}, \tag{3.8}$$

where A_j and B_j are dimensionless constants to be determined. Substituting $\vartheta = \vartheta_j$ and Eq. (3.8) into the second-order governing equation (Eq. (3.7)), the nonlinear displacement solutions can be obtained as:

$$w_j = C_j r + \frac{D_j r_{j-1}^2}{r} + \frac{B_j^2(\lambda + 3\mu + 2m)r_{j-1}^4}{2(\lambda + 2\mu)r^3}, \tag{3.9}$$

where C_j and D_j are dimensionless constants to be determined. Note that $B_1 = D_1 = 0$ in order to fulfill the nonsingular displacement condition u and w at $r = 0$. Also, for $j = 1$ the inner radius of the core $r_{j-1} = r_0 = 0$. There remain $4N - 2$ unknown dimensionless parameters A_1, C_1 and A_j, B_j, C_j, D_j, $j = 2, N$. These parameters depend on $\lambda_j, \mu_j, l_j, m_j$, the layer thicknesses $r_j - r_{j-1}$, $j = 1, N$ and the dilatations ϑ_j.

Substituting these solutions of displacement into Eqs. (3.3) and (3.5), the radial and circumferential stresses in each layer j can be written as:

$$T_{rj}^L = 2(\lambda_j + \mu_j)(A_j - \vartheta_j) - 2B_j\mu_j\frac{r_{j-1}^2}{r^2}, \tag{3.10}$$

$$T_{\varphi j}^L = 2(\lambda_j + \mu_j)(A_j - \vartheta_j) + 2B_j\mu_j\frac{r_{j-1}^2}{r^2}, \tag{3.11}$$

$$T_{rj}^{NL} = \frac{1}{(\lambda_j + 2\mu_j)r^4}(H_{1j} + H_{2j}r^2 + H_{3j}r^4), \tag{3.12}$$

$$T_{\varphi j}^{NL} = \frac{1}{(\lambda_j + 2\mu_j)r^4}(-3H_{1j} - H_{2j}r^2 + H_{3j}r^4), \tag{3.13}$$

where

$$H_{1j} = -(\lambda_j + 3\mu_j + 2m_j)\mu_j B_j^2 r_{j-1}^4, \tag{3.14}$$

$$H_{2j} = 2(\lambda_j + 2\mu_j)r_{j-1}^2(-D_j\mu_j - (\lambda_j + 3\mu_j + 2m_j)B_j(A_j - \vartheta_j)), \tag{3.15}$$

$$H_{3j} = (\lambda_j + 2\mu_j)(2C_j(\lambda_j + \mu_j) + (3\lambda_j + 3\mu_j + 2m_j + 4l_j)(A_j - \vartheta_j)^2). \tag{3.16}$$

Eqs. (3.8)–(3.16) are all power-law expressions. To solve for the $4N-2$ constants, the continuity of u_r across the interfaces at r_j, $j = 1, N-1$ requires:

$$u_j(r_j) = u_{j+1}(r_j), \quad w_j(r_j) = w_{j+1}(r_j) \quad j = 1,\ N-1, \tag{3.17}$$

while the continuity of T_r at the same interfaces requires:

$$T^L_{r_j}(r_j) = T^L_{r_{j+1}}(r_j), T^{NL}_{r_j}(r_j) = T^{NL}_{r_{j+1}}(r_j) \quad j = 1,\ N-1, \tag{3.18}$$

Finally, the traction-free condition at the outmost surface requires:

$$T^L_{r_N}(r_N) = T^{NL}_{r_N}(r_N) = 0. \tag{3.19}$$

These constitute a set of $4N-2$ equations which permit the solution for the same number of constants. The $4N-2$ constants take very complex forms. For a bilayer cylinder, the six constants are written out explicitly in Appendix B.

4. Numerical results

The objective of the numerical study is to investigate the tunability of the stresses and displacements, particularly the influence of elastic inhomogeneity, interface positions (or thickness inhomogeneity) and dilatation profile. Homogeneous, bilayer and four-layer cylinders are considered. Unless otherwise stated, the layers are of equal thickness $(r_j - r_{j-1})/r_1 = 1, j = 1, N$. The elastic constants used for the numerical results are based on the earlier works (Wu and Kirchner, 2010, 2011; Catheline et al., 2003) and are listed in Table 1. For the constants expressed in terms of NkT (typically 10^{-5}–10^{-2} GPa), N is the number of polymer chains per unit volume of dry polymer, k the Boltzmann's constant and T the absolute temperature. Two different dilatation profiles, step-up and step-down, are considered.

4.1. Tunable displacement and stresses

Consider a periodic four-layered cylindrical composite with Layers 1 and 3, and Layers 2 and 4, identical respectively. All layers are of equal thickness, such that $(r_j - r_{j-1})/r_1 = 1, j = 1, 4$. The elastic constants are $\lambda_1 = 3570\ NkT$, $\mu_1 = 1030\ NkT$, $l_1 = l_2 = 3560\ NkT$, $m_1 = -2420\ NkT$; the remaining ones will be varied. The step-up dilation profile is denoted by ϑ_{p1} with $\vartheta_1 = 0.1$, $\vartheta_2 = 0.2$, $\vartheta_3 = 0.3$ and $\vartheta_4 = 0.4$. Fig. 1 plots the surfaces of constant u_r at the outermost boundary, i.e., $u_r(r = r_4)/r_1 = 1.3,\ 1.6,\ 3$ in the $\lambda_2 - \mu_2 - m_2$ space. Essentially, this quantity typifies the amount of swelling when subjected to the specific dilatation. Several observations can be made as follows.

First, the bounds on λ_2, μ_2, m_2 can be estimated if u_r is to lie within or outside a certain range. For instance, if u_r is to be greater than 1.6, then λ_2, μ_2 and m_2 should be selected from the space under the middle surface represented by $u_r(r = r_4)/r_1 = 1.6$. These results suggest that the elasticity of the gels can be tuned to achieve a targeted functionality. In practice, gel stiffness can be varied over several orders of magnitude via cross-linking, photochemical modulation and other means (Engler et al., 2006; Kloxin et al., 2010).

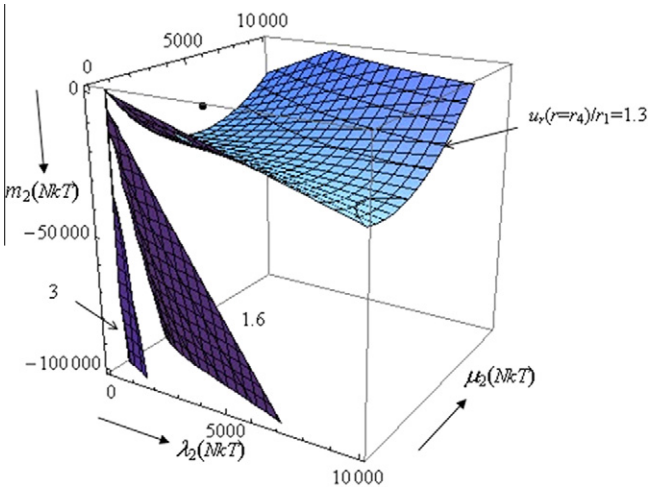

Fig. 2. The $\lambda_2 - \mu_2 - m_2$ surfaces of equal radial displacement $u_r(r = r_4)/r_1 = 1.3,\ 1.6,\ 3$ for a four-layer hydrogel cylinder subjected to a dilatation profile ϑ_{p1}. The dot represents a homogeneous cylinder.

Second, the surface shrinks in size and moves towards the vertical m_2 axis with increasing swelling. On the smaller and steeper surfaces, λ_2, μ_2 assume small values while m_2 may have large values. High compliance is characterized by small values of λ_2 and μ_2 ("linearly soft"), while high second-order nonlinear compliance is characterized by large negative values of m_2 ("nonlinearly soft"). Thus m_2, in addition to the second-order elastic constants, can be effectively used to modify the swelling response. It is also more difficult to achieve large swelling as the surface shrinks and steepens with increase in the radial displacement.

Third, Fig. 2 shows the advantage of layer inhomogeneity in a composite over homogeneity in a single-material cylinder. The dot in Fig. 2 locates the point where all the elastic constants of Layers 2 and 4 are identical to those of Layers 1 and 3. The corresponding value of $u_r(r = r_4)/r_1$ is 1.246 for this homogeneous cylinder. It appears that larger swelling can be achieved by increasing the layer inhomogeneity.

Using the same dilatation profile and the same fixed elastic constants as in Fig. 2, the dependence of the interfacial radial stress $T_r(r = r_1)/NkT$ on λ_2, μ_2 and m_2 is illustrated in Fig. 3. The surfaces correspond to the stress values of 300, 0 and −300, respectively. The dot refers to the homogeneous cylinder. The figure shows theoretically how both the stress magnitude and sign can be tuned. The middle surface is a zero radial stress surface, which partitions the space into tensile and compressive regions. The elastic constants corresponding to zero or small compressive stresses may be desirable, as tensile stresses encourage interfacial delamination while large compressive stresses may cause instability of the gel.

Table 1
Elastic constants for Figs. 2–8 (unit for Figs. 2–6 and Fig. 8: NkT, unit for Fig. 7: kPa).

Figure	λ_1	μ_1	l_1	m_1	λ_2	μ_2	l_2	m_2
2	3570	1030	−3560	−2420			−3560	
3	3570	1030	−3560	−2420			−3560	
4	35700	10.3	−3560	−2420	357		−100,000/−500	−2420
5	$35{,}700 \times 10^{\alpha}$	$10{,}300 \times 10^{\alpha}$	−3560	$-2420/10^{\alpha}$	$357/10^{\alpha}$	$103/10^{\alpha}$	−3560	$-242{,}000 \times 10^{\alpha}$
6	35,700	10,300	−3560	−242	357	103	−3560	−24,200
7	22.5×10^6	80	-2×10^6	-2×10^6	-0.225×10^6	0.8	-2×10^6	-200×10^6
8	3570	1030	−3560	−2420	3570	1030	−3560	−2420

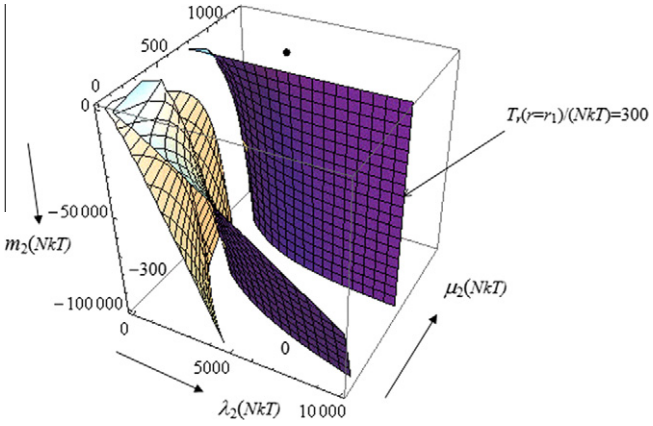

Fig. 3. The $\lambda_2-\mu_2-m_2$ surfaces of equal radial stress $T_r(r=r_1)/NkT=-300,\ 0,\ 300$ for a four-layer hydrogel cylinder subjected to a dilatation profile ϑ_{p1}. The dot represents a homogeneous cylinder.

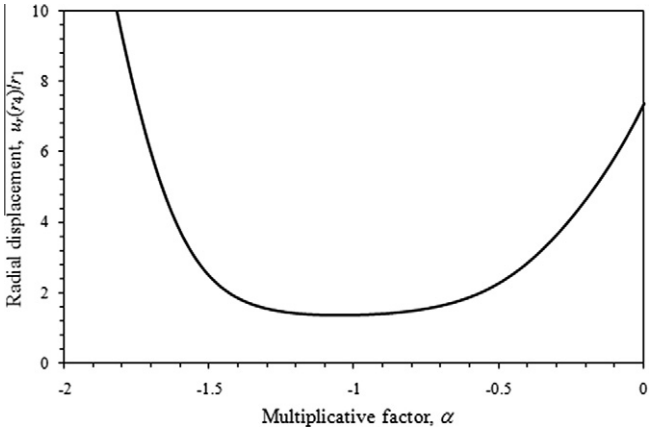

Fig. 5. Variation of the normalized radial displacement at the outer boundary of a four-layer cylinder subjected to the dilatation profile ϑ_{p1} with the multiplicative factor α for the elastic constants. The cylinder is homogeneous when $\alpha=-1$.

Within the range of λ_2, μ_2 and m_2 shown in the figure, it is not apparent that the surfaces shrink significantly as the radial stress evolves from tensile to compressive. However, the closer proximity of the surfaces representing zero and compressive stress implies a greater stress sensitivity to elastic parameter control in compression than in tension.

The radial stress at the position of r_1 in the homogeneous cylinder is tensile, with a magnitude of 356. Thus, the possibility of using layer inhomogeneity to effectively control the stress magnitude and sign is demonstrated in this figure.

By comparing Figs. 2 and 3, It is interesting to note that a larger swelling is associated with a compressive interfacial radial stress between Layers 1 and 2. However, the detailed stress characteristics may vary with the form of the dilatation profile and the elastic constants, as will be shown subsequently.

4.2. Influence of elastic constants

For Fig. 4, a bilayer cylinder is considered. The elastic constants are given by $\lambda_1=35700\,NkT$, $\mu_1=10.3\,NkT$, $l_1=-3560\,NkT$, $m_1=-2420\,NkT$, and $\lambda_2=357\,NkT$, $m_2=-2420\,NkT$. The applied dilatation profile is $\vartheta_1=0$ and $\vartheta_2=0.5$. The figure plots surface displacement $u_r(r=r_2)/r_1$ against μ_2 for two values of l_2, i.e., -500 and $-100{,}000\,NkT$. The results show that l_2 can also be used for controlling the swelling of the composite. The non-monotonous variation also suggests that a complex coupling exists between the elastic constants.

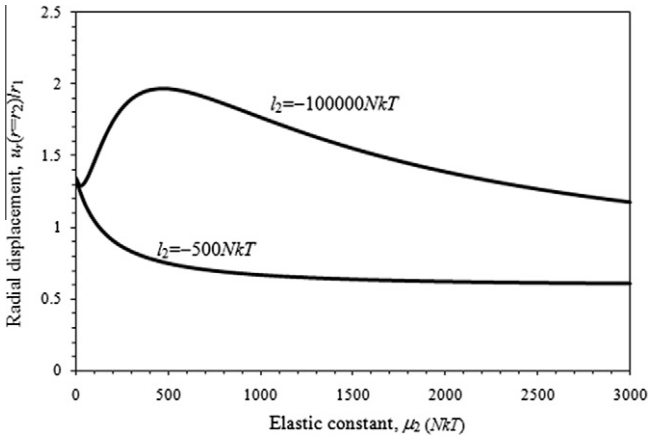

Fig. 4. Variation of the normalized radial displacement at the outer boundary with the shear modulus μ_2 for different values of l_2 in a bilayer hydrogel cylinder.

To illustrate the effect of elastic inhomogeneity, consider a periodic four-layer composite with identical Layers 1 and 3, and identical Layers 2 and 4, respectively. The layers are of the same thickness: $(r_j-r_{j-1})/r_1=1$, $j=1,\ 4$. The composite is loaded by the step-up dilatation profile ϑ_{p1}. Fig. 5 plots the outermost displacement $u_r(r=r_4)/r_1$ against a multiplicative factor α of the elastic constants, given by: $\lambda_1=35700\times10^{\alpha}\,NkT$, $\mu_1=10300\times10^{\alpha}\,NkT$, $l_1=-3560\,NkT$, $m_1=-2420/10^{\alpha}\,NkT$ for Layer 1, and $\lambda_2=357/10^{\alpha}\,NkT$, $\mu_2=103/10^{\alpha}\,NkT$, $l_2=-3560\,NkT$, $m_2=-242000\times10^{\alpha}\,NkT$ for Layer 2. As α increases from -2 to 0, Layers 1 and 3 become more linearly and nonlinearly stiff, while Layers 2 and 4 become more linearly and nonlinearly soft. It can be seen that the outermost displacement varies significantly with the elastic inhomogeneity. In fact, minimum swelling occurs when $\alpha\approx-1$, i.e., the composite is almost homogeneous, while larger swelling is associated with strong layer dissimilarity. These results suggest that it may be possible to control the swelling by properly designing the linear and nonlinear elasticity of the different layers of the composite.

To illustrate the relative importance of the nonlinear and linear effect, the ratio of nonlinear to linear circumferential stress $T_{\varphi}^{NL}/T_{\varphi}^{L}$ at the surface $r=r_4$ of a periodic four-layer cylinder with equal layer thickness is plotted against λ_2, μ_2, l_2, m_2 in Fig. 6. The dilatation profile is also ϑ_{p1}. The elastic constants, shown in Table 1,

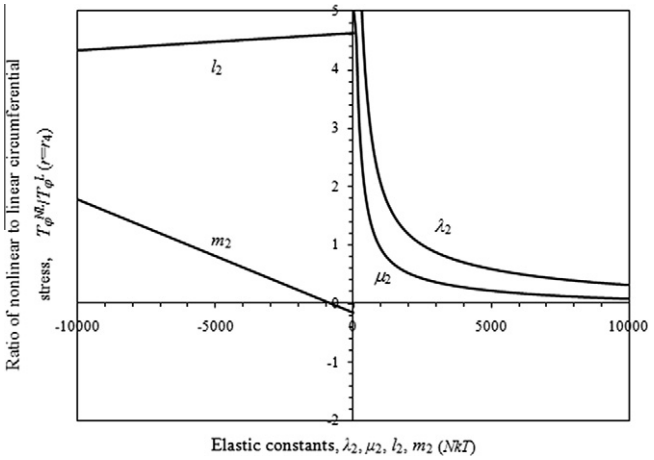

Fig. 6. Variation of the ratio of nonlinear to linear circumferential stress at the surface $r=r_4$ with λ_2, μ_2, l_2 and m_2 for a four-layer cylinder subjected to the dilatation profile ϑ_{p1}.

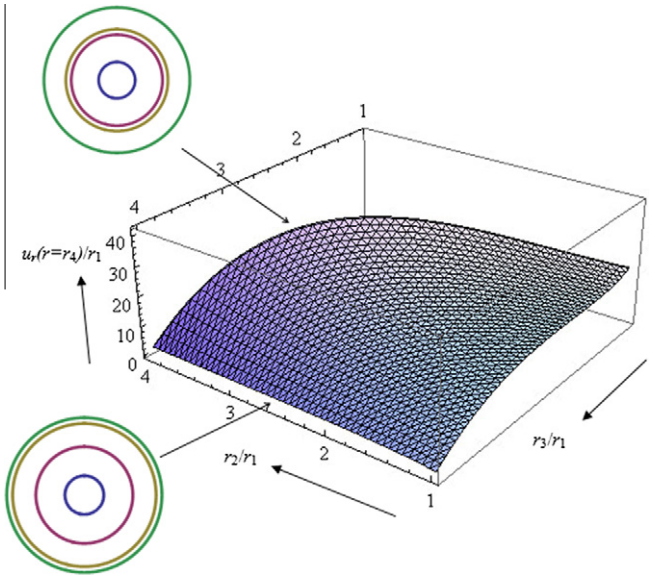

Fig. 7. Dependence of the surface displacement on r_2 and r_3 (r_1 and $r_4 = 4r_1$ fixed) for a four-layer hydrogel cylinder subjected to the dilatation profile ϑ_{p1}.

indicate that Layers 2 and 4 are more compliant (linearly and nonlinearly) than Layers 1 and 3. For each curve labeled by the constant λ_2, μ_2, l_2 or m_2, the constant is varied independently, keeping all the remaining seven constants fixed at the values indicated in Table 1. It can be observed that the stress ratio is rather large for most values of the varied constants, supporting the intuition that nonlinear components of stresses in soft materials can be dominant.

4.3. Influence of interface position

The effect of modifying the layer thickness of a periodic four-layer composite (with Layers 1 and 3, and Layers 2 and 4, identical in material respectively) is also investigated. Fig. 7 plots the variation of $u_r(r = r_4)/r_1$ versus r_2/r_1 and r_3/r_1, holding r_1 and $r_4 = 4r_1$ fixed. The dilatation profile is ϑ_{p1}. The elastic constants used for the simulations are suggested by the experimental data of Catheline et al. (2003) for agar-gelatin (a model for soft-tissue), in which λ is four to five orders of magnitude larger than μ. A maximum in u_r occurs when r_2/r_1 is slightly less than 3 and r_3/r_1 is slightly larger than 3. Hence, the composite with maximum swelling will resemble the configuration indicated in Fig. 7, which shows the "near-elimination" of the stiff Layer 3, resulting in a bilayer with unequal layer thicknesses. In contrast, if a small swelling is desired, Fig. 7 suggests a configuration with near-elimination of the compliant Layer 4 but with no specific requirement for the thickness of Layer 2. In general, larger swelling appears to be more easily obtained by changing the layer thicknesses than the elastic constants (compare Figs. 7 and 2). It should be mentioned that the dependence of such maximum/minimum swelling response on the interface positions is also evident when the values of λ and μ are comparable.

4.4. Influence of dilatation profile

In order to explore the effect of different dilatation profiles, the radial displacement, radial stress and circumferential stress are plotted against the radial coordinate in a *homogeneous* cylinder, as shown in Fig. 8. The elastic constants are given in Table 1. The two dilatation profiles are ϑ_{p1} and ϑ_{p2}, where the latter is a step-down profile with $\vartheta_1 = 0.4$, $\vartheta_2 = 0.3$, $\vartheta_3 = 0.2$ and $\vartheta_4 = 0.1$. In the current simulation, the dilatations are constant in the regions $0 \leqslant r \leqslant r_1$, $r_1 \leqslant r \leqslant r_2$, $r_2 \leqslant r \leqslant r_3$, $r_3 \leqslant r \leqslant r_4$.

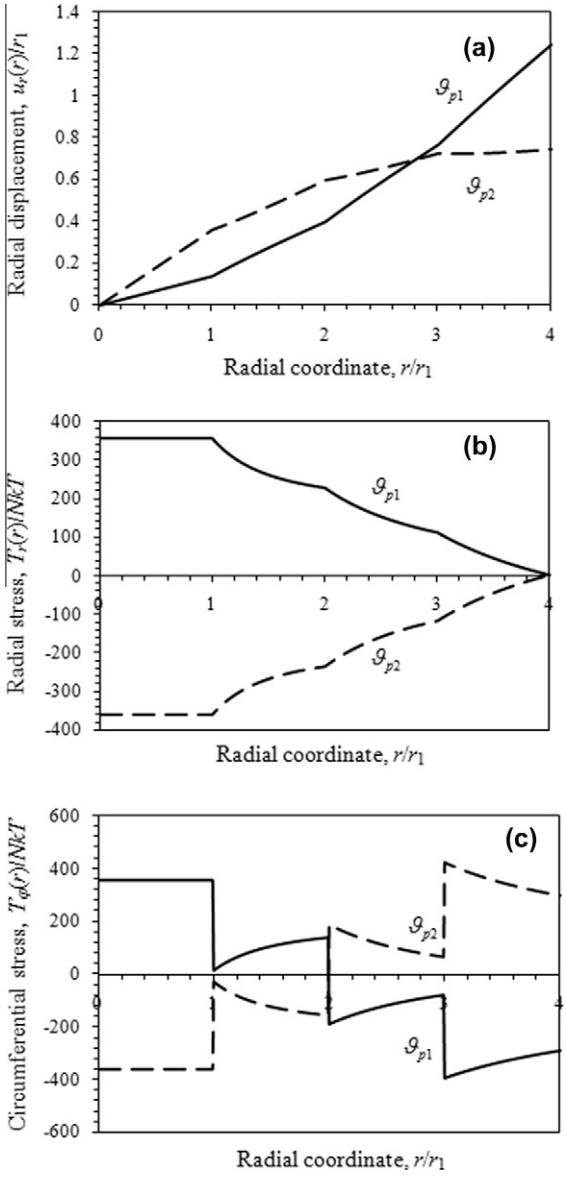

Fig. 8. Variation of the normalized (a) radial displacement, (b) radial stress and (c) circumferential stress with normalized radial coordinate r/r_1 in a homogeneous cylinder subjected to step-up (ϑ_{p1}) and step-down (ϑ_{p2}) dilatation profiles.

Several observations can be made. First, the radial displacement and radial stress are both continuous across the dilatation steps, while the circumferential stress is not. The radial displacement also changes linearly in each region, with a larger gradient for a larger dilatation, as shown in Fig. 8(a). The step-up profile also results in a larger swelling than the step-down profile. Figs. 8(b) and (c) show that the stresses generated by the two dilatation profiles are essentially opposite of each other. For instance, the radial stress produced by a step-down profile is compressive, since the material in the outer regions expands less than that in the inner regions. In general, the results show that the stress polarity can be influenced by the dilation profile alone, keeping in mind that the cylinder is entirely homogeneous. Hence, the design of a composite cylinder should take into consideration multiple factors (dilatation profile, layer elasticities, layer thicknesses) which influence the displacement and stresses in a coupled and complex manner. The continuum solutions presented here offer relatively simple "design

guidelines", which may not be easily obtained by computation-intensive models such as those based on microstructural details.

5. Conclusions

This paper develops solutions for a multilayered cylindrical gel subjected to step-up and step-down dilatation profiles in the framework of second-order elasticity. The displacement and stress solutions all assume the form of a power law with parameters dependent on the elastic constants, thickness and the dilation of each layer. The solutions emphasize the significant role of nonlinearity, elastic dissimilarity, layer thickness inhomogenity as well as the dilatation profile in the elastic fields. In particular, they show that a rational basis is possible for the mechanics design of complex bio-inspired materials, drug delivery vehicles and soft composites in general. For instance, the development of a multiaxial stress state conducive to successful cell culture in a bio-mimetic micro-environment may be established with the assistance of such theoretical calculations.

Appendix A

The derivation of the Jacobian stated in Eq. (2.6) is outlined here. Consider a circular tube deforming under the restriction of circular symmetry, i.e., each point in the tube undergoes a radial displacement $u_r(r)$, where r is the radial coordinate in the plane polar coordinate system (r, θ). According to Murnaghan (1951), $u_r(r)$ is replaced by $ku_r(r)$, where k keeps track of the order of approximation of the physical quantities. In the linear theory, terms up to the first power of k are retained, while in the second-order theory, terms up to the second powers of k are retained.

If **a** and **x(a)** denote the position vectors in the undeformed and deformed states of the sphere, respectively, then their differentials are:

$$d\mathbf{a} = \begin{pmatrix} dr \\ rd\theta \end{pmatrix}, \quad \mathbf{dx} = \begin{pmatrix} dr + kdu_r \\ (r + ku_r)d\theta \end{pmatrix}. \tag{A.1}$$

It can be easily seen that the differentials are related by the deformation gradient $\mathbf{J_a}$:

$$d\mathbf{x} = \mathbf{J}_\mathrm{a} d\mathbf{a}, \quad \mathbf{J}_\mathrm{a} = \mathrm{diag}\left[1 + ku_r', 1 + \frac{ku_r}{r}\right], \tag{A.2}$$

where "diag" denotes a 2 by 2 diagonal matrix and the prime denotes a derivative with respect to r. The second part of Eq. (A.2) is written as Eq. (2.6). The Lagrangian strain **E** then follows from the definition given in Eq. (2.7).

Appendix B

The six constants appearing in Eqs. (3.8)–(3.16) for a bilayer cylindrical composite gel are listed in the following:

$$A_1 = \frac{r_2^2(\lambda_2+\mu_2)(\vartheta_1\lambda_1+\vartheta_1\mu_1+\vartheta_2\mu_2)+r_1^2\mu_2(\vartheta_1\lambda_1+\vartheta_1\mu_1-\vartheta_2\lambda_2-\vartheta_2\mu_2)}{r_1^2(\lambda_1-\lambda_2+\mu_1-\mu_2)\mu_2+r_2^2(\lambda_2+\mu_2)(\lambda_1+\mu_1+\mu_2)}, \tag{B.1}$$

$$A_2 = \frac{-r_2^2\vartheta_2(\lambda_2+\mu_2)(\lambda_1+\mu_1+\mu_2)-r_1^2\mu_2(\vartheta_1\lambda_1+\vartheta_1\mu_1-\vartheta_2\lambda_2-\vartheta_2\mu_2)}{r_1^2(\lambda_1-\lambda_2+\mu_1-\mu_2)\mu_2+r_2^2(\lambda_2+\mu_2)(\lambda_1+\mu_1+\mu_2)}, \tag{B.2}$$

$$B_2 = \frac{r_2^2(\vartheta_1-\vartheta_2)(\lambda_1+\mu_1)(\lambda_2+\mu_2)}{r_1^2(\lambda_1-\lambda_2+\mu_1-\mu_2)\mu_2+r_2^2(\lambda_2+\mu_2)(\lambda_1+\mu_1+\mu_2)}, \tag{B.3}$$

$$C_1 = \frac{C_{11}+C_{12}+C_{13}+C_{14}}{C_{1D}}, \tag{B.4}$$

$$C_2 = \frac{C_{21}+C_{22}}{C_{2D}}, \tag{B.5}$$

$$D_2 = \frac{D_{21}+D_{22}}{D_{2D}}, \tag{B.6}$$

where:

$$C_{11} = -r_2^2\lambda_2(4l_1r_2^2\vartheta 1^2 + 2m_1r_2^2\vartheta_1^2 + 4B_2m_2r_1^2\vartheta_2 - 4B_2m_2r_2^2\vartheta_2 + 3r_2^2\vartheta_1^2\lambda_1 + 2B_2r_1^2\vartheta_2\lambda_2 - 2B_2r_2^2\vartheta_2\lambda_2 + 3r_2^2\vartheta_1^2\mu_1), \tag{B.7}$$

$$C_{12} = B_2^2r_1^2(r_1-r_2)(r_1+r_2)\mu_2(2m_2+\lambda_2) + 4B_2r_2^2(-r_1^2 + r_2^2)\vartheta_2\mu_2(m_2+2\lambda_2), \tag{B.8}$$

$$C_{13} = -r_2^2\mu_2(4l_1(r_1^2+r_2^2)\vartheta_1^2 + 2m_1(r_1^2+r_2^2)\vartheta_1^2 - 4l_2r_1^2\vartheta_2^2 - 2m_2r_1^2\vartheta_2^2 + 4l_2r_2^2\vartheta_2^2 + 2m_2r_2^2\vartheta_2^2 + 3r_1^2\vartheta_1^2\lambda_1 + 3r_2^2\vartheta_1^2\lambda_1 - 3r_1^2\vartheta_2^2\lambda_2 + 3r_2^2\vartheta_2^2\lambda_2 + 3(r_1^2+r_2^2)\vartheta_1^2\mu_1), \tag{B.9}$$

$$C_{14} = 3(r_1-r_2)(r_1+r_2)(B_2^2r_1^2 - 2B_2r_2^2\vartheta_2 + r_2^2\vartheta_2^2)\mu_2^2 + A_2^2(r_1 - r_2)r_2^2(r_1+r_2)\mu_2(4l_2+2m_2+3\lambda_2+3\mu_2) - A_1^2r_2^2(4l_1+2m_1+3\lambda_1+3\mu_1)(r_1^2\mu_2+r_2^2\lambda_2+r_2^2\mu_2) + 2A_1r_2^2\vartheta_1(4l_1+2m_1+3\lambda_1+3\mu_1)(r_1^2\mu_2+r_2^2\lambda_2 + r_2^2\mu_2) + 2A_2(r_1-r_2)r_2^2(r_1+r_2)(B_2(\lambda_2+\mu_2)(2m_2 + \lambda_2+3\mu_2) - \vartheta_2\mu_2(4l_2+2m_2+3\lambda_2+3\mu_2)), \tag{B.10}$$

$$C_{1D} = 2r_1^2r_2^2(\lambda_1-\lambda_2+\mu_1-\mu_2)\mu_2 + 2r_2^4(\lambda_2+\mu_2)(\lambda_1+\mu_1+\mu_2), \tag{B.11}$$

$$C_{21} = -B_2^2r_1^2(r_1-r_2)(r_1+r_2)\mu_2(\lambda_1+\mu_1+\mu_2)(2m_2+\lambda_2 + 3\mu_2) + 2B_2r_1^2r_2^2\vartheta_2(\lambda_1+\mu_1)(\lambda_2+2\mu_2)(2m_2+\lambda_2 + 3\mu_2) + A_2^2r_2^2(-r_1^2\mu_2+r_2^2\lambda_1+r_2^2\mu_1+r_2^2\mu_2)(\lambda_2 + 2\mu_2)(4l_2+2m_2+3\lambda_2+\mu_2) - 2A_2B_2r_1^2r_2^2(\lambda_2 + 2\mu_2)(\lambda_1+\mu_1)(2m_2+\lambda_2+3\mu_2) - 2A_2\vartheta_2r_2^2(-r_1^2\mu_2 + r_2^2\lambda_1+r_2^2\mu_1+r_2^2\mu_2)(\lambda_2+2\mu_2)(4l_2+2m_2+3\lambda_2+3\mu_2), \tag{B.12}$$

$$C_{22} = r_2^2(\lambda_2+2\mu_2)((A_1-\vartheta_1)^2r_1^2(4l_1+2m_1)\mu_2 + \vartheta_2^2(-r_1^2\mu_2 + r_2^2\lambda_1+r_2^2\mu_1+r_2^2\mu_2)(4l_2+2m_2) + 3\vartheta_2^2r_2^2(\lambda_2+\mu_2) \times(\lambda_1+\mu_1+\mu_2) + 3(A_1-\vartheta_1)^2r_1^2\mu_2(\lambda_1+\mu_1) - 3r_1^2\mu_2\vartheta_2^2(\lambda_2+\mu_2)), \tag{B.13}$$

$$C_{2D} = -2r_1^2r_2^2(\lambda_2+2\mu_2)(\lambda_1-\lambda_2+\mu_1-\mu_2)\mu_2 - 2r_2^4(\lambda_2 + 2\mu_2)(\lambda_2+\mu_2)(\lambda_1+\mu_1+\mu_2), \tag{B.14}$$

$$D_{21} = \frac{(\lambda_2+\mu_2)}{\lambda_2+2\mu_2}2r_1r_2^2((B_2^2(\lambda_1+\mu_1+\mu_2)(2m_2+\lambda_2+3\mu_2) + 2B_2(A_2-\vartheta_2)(\lambda_2+2\mu_2)(2m_2+\lambda_2+3\mu_2) + (\lambda_2 + 2\mu_2)(A_1-\vartheta_1)^2(4l_1+2m_1+3\lambda_1+3\mu_1) - (\lambda_2 + 2\mu_2)(A_2-\vartheta_2)^2(4l_2+2m_2+3\lambda_2+3\mu_2)), \tag{B.15}$$

$$D_{22} = 2r_1r_2^2(\lambda_1-\lambda_2+\mu_1-\mu_2) \left(\frac{2B_2r_1^2\vartheta_2(2m_2+\lambda_2+3\mu_2)}{r_2^2} - \frac{B_2^2r_1^4\mu_2(2m_2+\lambda_2+3\mu_2)}{r_2^4(\lambda_2+2\mu_2)} + (A_2-\vartheta_2)^2(4l_2+2m_2+3\lambda_2+3\mu_2) - \frac{2A_2B_2r_1^2(2m_2+\lambda_2+3\mu_2)}{r_2^2}\right), \tag{B.16}$$

$$D_{2D} = -4r_1^3(\lambda_1-\lambda_2+\mu_1-\mu_2)\mu_2 - 4r_1r_2^2(\lambda_2+\mu_2)(\lambda_1+\mu_1+\mu_2). \tag{B.17}$$

References

Catheline, S., Gennisson, J.L., Fink, M., 2003. Measurement of elastic nonlinearity of soft solid with transient elastography. J. Acoust. Soc. Am. 114, 3087–3091.

Destrade, M., Gilchrist, M.D., Ogden, R.W., 2010. Third- and fourth-order elasticities of biological soft tissues. J. Acoust. Soc. Am. 127, 2103–2106.

Engler, A.J., Sen, S., Sweeney, H.L., Discher, D.E., 2006. Matrix elasticity directs stem cell lineage specification. Cell 126, 677–689.

Facca, S., Cortez, C., Mendoza-Palomares, C., Messadeq, N., Dierich, A., Johnston, A.P.R., Mainard, D., Voegel, J.C., Caruso, F., Benkirane-Jessel, N., 2010. Active multilayered capsules for in vivo bone formation. P. Nat. Acad. Sci. USA 107, 3406–3411.

Johnson, L.M., DeForest, C.A., Pendurti, A., Anseth, K.S., Bowman, C.N., 2010. Formation of three-dimensional hydrogel multilayers using enzyme-mediated redox chain initiation. ACS Appl. Mater. Inter. 2, 1963–1972.

Kloxin, A.M., Benton, J.A., Anseth, K.S., 2010. In situ elasticity modulation with dynamic substrates to direct cell phenotype. Biomaterials 31, 1–8.

Marklein, R.A., Burdick, J.A., 2010. Controlling stem cell fate with material design. Adv. Mater. 22, 175–189.

Murnaghan, F.D., 1951. Finite Deformation of An Elastic Solid. John Wiley, New York.

Rénier, M., Gennisson, J.L., Barriere, C., Royer, D., Fink, M., 2008. Fourth-order shear elastic constant assessment in quasi-incompressible soft solids. Appl. Phys. Lett. 93.

Schneider, S., Feilen, P.J., Slotty, V., Kampfner, D., Preuss, S., Berger, S., Beyer, J., Pommersheim, R., 2001. Multilayer capsules: a promising microencapsulation system for transplantation of pancreatic islets. Biomaterials 22, 1961–1970.

Wang, D., Wu, M.S. 2012. Analytical solutions for bilayered spherical hydrogel subjected to constant dilatation. Accepted for publication.

Wu, M.S., Kirchner, H.O.K., 2010. Nonlinear elasticity modeling of biogels. J. Mech. Phys. Solids 58, 300–310.

Wu, M.S., Kirchner, H.O.K., 2011. Second-order elastic solutions for spherical gels subjected to spherically symmetric dilatation. Mech. Mater. 43, 721–729.